Journal of Physics: Conference Series **362** (2012) 012034 doi:10.1088/1742-6596/362/1/012034

Heat transfer in micro devices packaged in partial vacuum

Anirudh Rana[1], Manuel Torrilhon[2], Henning Struchtrup[1]

[1]Department of Mechanical Engineering,
University of Victoria, Victoria BC, Canada
[2]Department of Mathematics,
RWTH Aachen University, Aachen, Germany

E-mail: anirudh@uvic.ca

Abstract. The influence of rarefaction effects on technical processes is studied numerically for a heat transfer problem in a rarefied gas, a box with bottom heated plate. Solutions obtained from several macroscopic models, in particular the classical Navier-Stokes-Fourier equations with jump and slip boundary conditions, and the regularized 13 moment (R13) equations [Struchtrup & Torrilhon, *Phys. Fluids* 15, 2003] are compared. The R13 results show significant flow patterns which are not present in the classical hydrodynamic description.

1. Introduction

Accurate prediction of gas flow through microfluidic devices is important to enable the optimum performance, design and fabrication of micro-electro-mechanical systems (MEMS). Simulation of the gas flow through these micro devices is, however, more challenging than in classical flow regimes, since gas rarefaction leads to the breakdown of the underlying assumptions of the classical continuum theory, i.e., the Navier-Stokes-Fourier (NSF) equations.

The state of a gas in such microsystems is described by the Knudsen number which is defined as $Kn = \frac{\lambda}{L}$, where L is the length scale of device and λ is the mean free path of gas molecules, given by $\frac{\mu}{\rho\sqrt{RT}}$. Here, μ is the dynamic viscosity, R is the gas constant and T and ρ are the temperature and density of the gas, respectively.

Based upon the value of Knudsen number, gas flows in micro devices can be categorized into three regimes. For $Kn \leq 10^{-3}$, the gas is considered as a continuum, while for $Kn \geq 10$ it is considered to be in the free molecular flow regime. For Knudsen numbers ranging between $10^{-3} \leq Kn \leq 10$, known as the transition regime, the gas exhibits rarefaction effects such as Knudsen layers, Knudsen minimum, heat flux without temperature gradient, thermal creep, etc. [2]-[5].

The transition regime is a challenging regime to model, and perhaps the one most frequently encountered in MEMS devices [6]. Many MEMS applications involve the analysis of gas flow through microdevices such as micro-Pirani gauges [7][8], microcantilever heaters [9][10], etc. In these microdevices, where the characteristic length scale of the device is comparable with the mean free path, the Knudsen number ceases to be sufficiently small for the NSF equations to hold.

Direct numerical solution of the Boltzmann equation gives an accurate microscopic description of gas flows at all Knudsen numbers, but requires detailed information on microscopic phase space, and thus typically huge computational times [11]. The direct simulation Monte Carlo (DSMC) method, proposed by Bird [12], is another commonly used numerical method for simulation of high Knudsen number gas flows. In MEMS, however, where the mean streamwise velocity is several orders of magnitude smaller than the mean molecular velocity $\left(\sqrt{2RT}\right)$, the DSMC method produces significant statistical noise. Normally, a large number of samples, and therefore huge computational times, are required to reduce the noise. Recently, several variants of the DSMC method were presented which have, for some flow problems, reduced computational time [13][14].

For the purpose of design optimization, which requires numerous repetition of simulations with different parameters, microscopic solvers are impractical due to the large computational time involved. Moreover, since the solution is produced in the microscopic picture, the underlying physics for a typical thermodynamic process remains somewhat hidden. Indeed, microscopic solvers consider the behavior of individual particles, but not their collective behavior. This makes it impossible to deduce, a priory, the relative size of relevant macroscopic physical quantities, e.g., density, temperature, heat flux, stress, and their relative effect on the particular process under consideration.

Beside microscopic approaches, a thermodynamic process can also be described by macroscopic models, derived from the Boltzmann kinetic equation either by asymptotic expansion, such as in the Chapman-Enskog expansion [15], or by reconstruction of the distribution function, such as in Grad's moment method [16]. In macroscopic theories, the behavior of a gas is described through physical quantities such as mass density, temperature, velocity, heat flux, stress tensor, and so on. The goal of these macroscopic models is to reduce the high dimensional phase space of the particle description to a low-dimensional continuum model by relating the physical quantities as moments of the probability density function $f(c, x, t)$. Macroscopic models, despite some limitation on the their accuracy, give an easy and detailed access to physical quantities and their relative effect on the process. In recent years, we developed the regularized 13 moment equations (R13), which give good predictions for rarefied flows with Knudsen numbers up to 0.5 [1][18]-[23].

In the present contribution we study the gas flow behaviour and heat transfer characteristics of a rarefied gas confined in a bottom heated square domain. A similar problem has been investigated using DSMC or another kinetic approaches in [9][24]-[30]. In the following we shall consider the effects of Knudsen number and convection on heat transfer from the heated plate using finite difference numerical solutions of macroscopic methods. The developed numerical method is applied to the R13 equations, and to the Navier–Stokes equations supplemented by the first and second order velocity-slip and temperature-jump conditions. The main objective here is the implementation of a computationally efficient yet accurate, macroscopic description of such flows, so as to anticipate a better understanding of heat transfer process in micro devices.

2. Statement of the Problem

We consider the steady state heat transfer process through a monatomic gas, trapped inside a square enclosure of width L with a uniformly heated surface at the bottom ($y = 0$), as shown in Fig. 1. It is assumed that the temperature of the heated surface of the cavity is T_H and the other sides are considered isothermal at an environment temperature $T_0 = 273K$. The ratio between hot chip surface temperature, T_H, and T_0 was taken to be 1.1. Results will be presented for Knudsen numbers ranging from the continuum limit to the early transition regime, i.e., $10^{-3} \leq Kn \leq 1$. Effects due to radiation and gravity are assumed to be negligible.

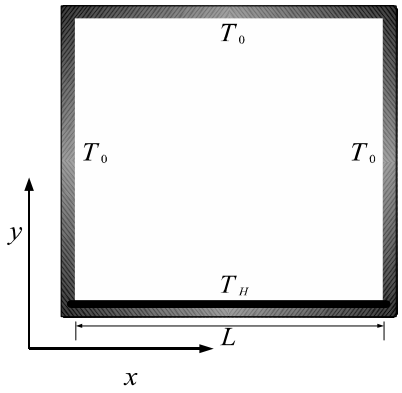

Figure 1. Schematic diagram for bottom heated plate.

3. Macroscopic Transport Equations

Macroscopic equations for rarefied gases are obtained by multiplying the Boltzmann equation with weight functions and integrating it over the velocity space. By taking appropriate weight functions, we obtain the conservation laws for mass, momentum, and energy [31],

$$\frac{\partial \rho}{\partial t} + \frac{\partial \rho v_i}{\partial x_i} = 0, \tag{1a}$$

$$\frac{\partial \rho v_i}{\partial t} + \frac{\partial \left(p_{ik} + \rho v_i v_k\right)}{\partial x_k} = 0, \tag{1b}$$

$$\frac{\partial \rho \left(u + \frac{1}{2}v^2\right)}{\partial t} + \frac{\partial \left(\rho e v_k + p_{ik} v_i + q_k\right)}{\partial x_k} = 0, \tag{1c}$$

where t and x_i are temporal and spatial coordinates, respectively. Moreover, ρ, v_k, p_{ik}, u, and q_k denote mass density, velocity, pressure tensor, internal energy density and the heat flux, along with

$$p_{ij} = p\delta_{ij} + \sigma_{ij} \quad \text{and } u = \frac{3\theta}{2}. \tag{2}$$

Here, p and σ_{ij} are the pressure and the stress tensor, respectively. Also, for ideal monatomic gases the pressure is given by the ideal gas law, $p = \rho\theta = \rho RT$, where θ is the temperature in energy units, R is the gas constant and T is the thermodynamic temperature.

Closure of the conservation laws (1a-1c) requires to specify the pressure tensor, p_{ij} and the heat flux vector, q_k. Several methods to this end can be found in the literature.

One approach to the closure of the macroscopic equations is given by a series expansion of the distribution function in terms of Knudsen number, the Chapman-Enskog (CE) expansion [15]. The Euler and the Navier-Stokes-Fourier equations result from the zeroth and first order expansions, respectively, while higher order expansions lead to the Burnett and Super-Burnett equations [32]. However, in many cases, the higher order CE expansion leads to unstable or unphysical results [33]. Moreover, there is no complete theory for boundary conditions of the higher order equations.

Another approach is due to Grad [16], known as the Grad's moment methods, in which the velocity distribution function is reconstructed by an expansion of the distribution function into Hermite polynomials. The method yields extended sets of transport equations, the best-known

of which is the 13 moment system. The Grad method is not linked to the Knudsen number, and thus it provides no information on which, and how many, moments one should consider for a given process.

The regularized-13 (R13) equations [1][31] were obtained by combining elements of the CE and Grad methods, they are a regularized version of the classical Grad's 13-moment equations. The R13 equations are of third order in the Knudsen number in the CE sense, and for small enough Knudsen numbers ($Kn \lesssim 0.5$) the equations describe all known rarefaction effects with good accuracy [19]-[22].

The equations for heat-flux vector and stress tensor in the R13 system are their respective moment equations

$$\frac{\partial q_i}{\partial t} + v_k\frac{\partial q_i}{\partial x_k} + \frac{7}{5}q_k\frac{\partial v_i}{\partial x_k} - \sigma_{ik}\frac{\theta}{\rho}\frac{\partial \rho}{\partial x_k} - \frac{\sigma_{ik}}{\rho}\frac{\partial \sigma_{kl}}{\partial x_l} + \frac{7}{2}\frac{\partial \theta\sigma_{ik}}{\partial x_k} + \frac{5}{2}\sigma_{ik}\frac{\partial \theta}{\partial x_k} + \theta\frac{\partial \sigma_{ik}}{\partial x_k} + \frac{7}{5}q_i\frac{\partial v_k}{\partial x_k} + \frac{2}{5}q_k\frac{\partial v_k}{\partial x_i} + \frac{1}{2}\frac{\partial R_{ik}}{\partial x_k} + \frac{1}{6}\frac{\partial \Delta}{\partial x_i} + m_{ikl}\frac{\partial v_k}{\partial x_l} + \underline{\frac{5}{2}p\frac{\partial \theta}{\partial x_i}} = \underline{-\frac{2}{3}\frac{p}{\mu}q_i}, \quad (3)$$

$$\frac{\partial \sigma_{ij}}{\partial t} + v_k\frac{\partial \sigma_{ij}}{\partial x_k} + \frac{\partial m_{ijk}}{\partial x_k} + \frac{4}{5}\frac{\partial q_{\langle i}}{\partial x_{j\rangle}} + 2\sigma_{k\langle i}\frac{\partial v_{j\rangle}}{\partial x_k} + \sigma_{ij}\frac{\partial v_k}{\partial x_k} + \underline{2p\frac{\partial v_{\langle i}}{\partial x_{j\rangle}}} = \underline{-\frac{p}{\mu}\sigma_{ij}}, \quad (4)$$

For $\Delta = R_{ij} = m_{ijk} = 0$, the above equations reduce to Grad's 13-moment equations [16]. The R13 closure for Δ, R_{ij} and m_{ijk} results from taking into account the appropriate terms of higher order moment equations, so that

$$\begin{aligned}
\Delta &= 5\frac{\sigma_{kl}\sigma_{kl}}{\rho} + \frac{56}{5}\frac{q_k q_k}{p} - 12\frac{\mu}{p}\left(\theta\frac{\partial q_k}{\partial x_k} - \theta q_k\frac{\partial \ln p}{\partial x_k}\right), \quad (5)\\
R_{ij} &= \frac{20}{7}\frac{\sigma_{k\langle i}\sigma_{j\rangle k}}{\rho} + \frac{192}{75}\frac{q_{\langle i}q_{j\rangle}}{p} - \frac{24}{5}\frac{\mu}{p}\left(\theta\frac{\partial q_{\langle i}}{\partial x_{j\rangle}} - \theta q_{\langle i}\frac{\partial \ln p}{\partial x_{j\rangle}}\right),\\
m_{ijk} &= \frac{20}{15}\frac{q_{\langle i}\sigma_{jk\rangle}}{p} - 2\frac{\mu}{p}\left(\theta\frac{\partial \sigma_{\langle ij}}{\partial x_{k\rangle}} - \theta\sigma_{\langle ij}\frac{\partial \ln p}{\partial x_{k\rangle}}\right).
\end{aligned}$$

The indices inside angular brackets denote the symmetric trace-free part of tensors [31]. The R13 constitutive relations given by eqs. (5) add second order derivatives to stress tensor, σ_{ij} and heat flux, q_i, in eqs. (3 and 4).

The R13 equations are an extension to the classical Navier-Stokes- Fourier (NSF) equations of hydrodynamics. An analysis of the order of Knudsen number in (3-4) shows that only the underlined terms are of first order in Knudsen number, while all others are of higher order [34]. Thus, the underlined terms are the NSF contributions,

$$q_i^{NSF} = -\frac{15}{4}\mu\frac{\partial \theta}{\partial x_i}, \text{ and } \sigma_{ij}^{NSF} = -2\mu\frac{\partial v_{\langle i}}{\partial x_{j\rangle}}\ . \quad (6)$$

From now on, all equations and results will be given in dimensionless quantities, defined as

$$\widehat{x_i} = \frac{x_i}{L},\ \widehat{\theta} = \frac{\theta}{\theta_0},\ \widehat{\rho} = \frac{\rho}{\rho_0},\ \widehat{v_i} = \frac{v_i}{\sqrt{\theta_0}},\ \widehat{q_i} = \frac{v_i}{\rho_0\sqrt{\theta_0}^3},$$
$$\widehat{\sigma_{ij}} = \frac{\sigma_{ij}}{\rho_0\theta_0},\ \hat{\Delta} = \frac{\Delta}{\varrho_0\,\theta_0^2},\ \hat{R}_{ij} = \frac{R_{ij}}{\varrho_0\,\theta_0^2},\ \text{and}\ \ \hat{m}_{ijk} = \frac{m_{ijk}}{\varrho_0\sqrt{\theta_0}^3}\ .$$

Here, ρ_0 is the average mass density. As a result the Knudsen number arises, which is given by

$$Kn = \frac{\mu_0}{\rho_0\sqrt{\theta_0}}\frac{1}{L},$$

where L is the length of the bottom wall. Therefore, the flow considered is fully defined by setting the temperature ratio T_H/T_0 and the Knudsen number.

3.1. Boundary conditions

Maxwell's accommodation model for the boundary conditions in kinetic theory was used to derive boundary conditions for the R13 system, which link the moments of the gas near the wall to the tangential wall velocity v_τ^W and wall temperature θ^W. The details of the construction procedure for the boundary conditions (BCs) for the R13 equations can be found in [17], the final result reads

$$v_n = 0 \tag{7a}$$

$$\sigma_{\tau n} = \frac{-\chi}{2-\chi}\sqrt{\frac{2}{\pi\theta}}\left(\mathcal{P}\mathcal{V}_\tau + \frac{1}{5}q_\tau + \frac{1}{2}m_{\tau nn}\right), \tag{7b}$$

$$q_n = \frac{-\chi}{2-\chi}\sqrt{\frac{2}{\pi\theta}}\left(2\mathcal{P}\mathcal{T} - \frac{1}{2}\mathcal{P}\mathcal{V}_\tau^2 + \frac{1}{2}\theta\sigma_{nn} + \frac{1}{15}\Delta + \frac{5}{28}R_{nn}\right), \tag{7c}$$

$$R_{\tau n} = \frac{\chi}{2-\chi}\sqrt{\frac{2}{\pi\theta}}\left(6\mathcal{P}\mathcal{T}\mathcal{V}_\tau + \mathcal{P}\theta\mathcal{V}_\tau - \mathcal{P}\mathcal{V}_\tau^3 - \frac{11}{5}\theta q_\tau - \frac{1}{2}\theta m_{\tau nn}\right), \tag{7d}$$

$$m_{nnn} = \frac{\chi}{2-\chi}\sqrt{\frac{2}{\pi\theta}}\left(\frac{2}{5}\mathcal{P}\mathcal{T} - \frac{3}{5}\mathcal{P}\mathcal{V}_\tau^2 - \frac{7}{5}\theta\sigma_{nn} + \frac{1}{75}\Delta - \frac{1}{14}R_{nn}\right), \tag{7e}$$

$$m_{\tau\tau n} = \frac{-\chi}{2-\chi}\sqrt{\frac{2}{\pi\theta}}\left(\frac{1}{5}\mathcal{P}\mathcal{T} - \frac{4}{5}\mathcal{P}\mathcal{V}_\tau^2 + \frac{1}{14}R_{\tau\tau} + \theta\sigma_{\tau\tau} - \frac{1}{5}\theta\sigma_{nn} + \frac{1}{150}\Delta\right), \tag{7f}$$

where

$$\mathcal{P} = \rho_W\sqrt{\theta_W}\sqrt{\theta} = \left(\rho\theta + \frac{1}{2}\sigma_{\tau\tau} - \frac{1}{120}\frac{\Delta}{\theta} - \frac{1}{28}\frac{R_{\tau\tau}}{\theta}\right). \tag{8}$$

Here, $\mathcal{V}_\tau = v_\tau - v_\tau^W$ and $\mathcal{T} = \theta - \theta_W$ are slip velocity and temperature jump, respectively, and subscripts n and τ stand for the normal and tangential directions with respect to the surface. The accommodation coefficient in the Maxwell model is denoted by χ, representing the fraction of molecules undergoing diffuse reflection. For all numerical results presented in this paper accommodation factor is set to be unity [2].

Equation (7b) relates the velocity slip $\mathcal{V}_\tau$, to the shear stress $\sigma_{\tau n}$, associated with the gradient of tangential velocity in the normal direction, and the heat flux q_τ, associated with the gradient of temperature parallel to the boundary. Therefore, in contrast to continuum flows, a tangential temperature gradient along the surface can also induce a flow from the colder part to the hotter part, usually referred to as thermal creep [2].

In the slip flow regime, the NSF equations must be furnished with slip and jump boundary conditions. Slip and jump boundary conditions for the Navier-Stokes-Fourier equations are obtained by replacing, $\sigma_{ij} = \sigma_{ij}^{NSF}$ and $q_i = q_i^{NSF}$ from Eqs. (6), in Eqs.(7a-7c) and ignoring higher order moments, i.e., $m_{\tau nn}$, Δ and R_{nn}. As a result we obtain [5]

$$v_n = 0 \tag{9a}$$

$$\sigma_{\tau n}^{NSF} = \frac{-\chi}{2-\chi}\sqrt{\frac{2}{\pi\theta}}\left(\mathcal{P}\mathcal{V}_\tau - \frac{3}{4}\mu\frac{\partial\theta}{\partial x_\tau}\right), \tag{9b}$$

$$q_n^{NSF} = \frac{-\chi}{2-\chi}\sqrt{\frac{2}{\pi\theta}}\left(2\mathcal{P}\mathcal{T} - \frac{1}{2}\mathcal{P}\mathcal{V}_\tau^2 - \mu\theta\frac{\partial v_{\langle n}}{\partial x_{n\rangle}}\right), \tag{9c}$$

where $\mathcal{P} = \left(\rho\theta + \frac{1}{2}\sigma_{\tau\tau}\right)$.

Second order slip and jump boundary conditions can also be derived from (7a-7c), by replacing the heat flux and stress using Navier-Stokes-Fourier constitutive relations (6) in higher order

moments, i.e., $m_{\tau nn}$, Δ and R_{nn} [5]

$$v_n = 0 \tag{10a}$$

$$\sigma_{\tau n}^{NSF} = \frac{-\chi}{2-\chi}\sqrt{\frac{2}{\pi\theta}}\left(\mathcal{P}\mathcal{V}_\tau + \frac{1}{5}q_\tau^{NSF} + \frac{1}{2}m_{\tau nn}^{NSF}\right), \tag{10b}$$

$$q_n^{NSF} = \frac{-\chi}{2-\chi}\sqrt{\frac{2}{\pi\theta}}\left(2\mathcal{P}\mathcal{T} - \frac{1}{2}\mathcal{P}\mathcal{V}_\tau^2 + \frac{1}{2}\theta\sigma_{nn}^{NSF} + \frac{1}{15}\Delta^{NSF} + \frac{5}{28}R_{nn}^{NSF}\right). \tag{10c}$$

Here, the superscript NSF denotes that the actual heat flux and stress are replaced using the Navier-Stokes-Fourier constitutive relations.

4. Results and discussion

To obtain the numerical solution a central finite-difference scheme was used and the system of discretized equations has been solved using a quasi-minimal residual method. This numerical algorithm has been described and validated against the existing results for the case of the lid driven cavity in [35]. The numerical algorithm converges with approximately second-order numerical accuracy, and a grid independent solution (with less then 1% deviation) was obtained approximately at 70×70 mesh size.

4.1. Rarefaction effects on flow field characteristics

Fig. 2(a)-(d) show the results for Knudsen numbers 0.06, 0.12, 0.335 and 0.5, respectively, for the temperature ratio $T_H/T_0 = 1.1$. The flow fields are symmetric to the centerline ($x = 0.5$); for compact presentation, the figures show NSF results (using 1st order BC) in the left part, and R13 results on the right. The figures show temperature contours and velocity streamlines.

As we see from Fig. 2, for all Kn, two primary circulating vortices are induced near the heated surface, along the vertical axes. The formation of primary vortices, is induced by the tangential temperature gradient in the gas near the vertical surface that forces a creep-driven fluid into a circulatory motion.

Interestingly, in addition of the primary vortices, the R13 equations predict a secondary counter-circulating flow induced along the corners of the top plate. These predictions are qualitatively similar to those seen in Monte Carlo simulations for vacuum packaged MEMS devices [27] and [38]. This flow behavior results form the interplay of the variables as given by the transport equations, and from the slip equation (7b), which relates the tangential velocity v_τ to shear stress, $\sigma_{\tau n}$, tangential heat flux, q_τ, and higher order contribution, $m_{\tau nn}$. The latter can be rearranged to give an expression for the tangential velocity at the right vertical surface as,

$$v_x \propto \left(\frac{2-\chi}{\chi}\sqrt{\frac{\pi\theta}{2}}\sigma_{xy} - \frac{1}{5}q_y - \frac{1}{2}m_{yxx}\right). \tag{11}$$

At moderate Knudsen numbers, the tangential velocity has two opposing contributions, one from the tangential heat flux, q_y and the second from the shear stress, σ_{xy}.

For example, on the right vertical surface, along $x = 1$ (see Fig. 1), the tangential heat flux, q_τ, is positive mainly due to a negative temperature gradient (Fourier law). The magnitude of q_τ increases with the Knudsen number (also with the temperature ratio), whereas it decreases as the gas moves further away from the bottom surface. Along the vertical surface, both the Navier-Stokes-Fourier (NSF) and the R13 equations predict positive shear stress. However, the Navier-Stokes equations under-predict the shear stress, $\sigma_{\tau n}$, in comparison to the R13 equations. In particular, the NSF equations do not take into account the thermal stress, i.e., $\sigma_{ij}^T \propto -\frac{\mu}{p}\frac{\partial q_{\langle i}}{\partial x_{j\rangle}}$, which appears in the stress balance equation (4).

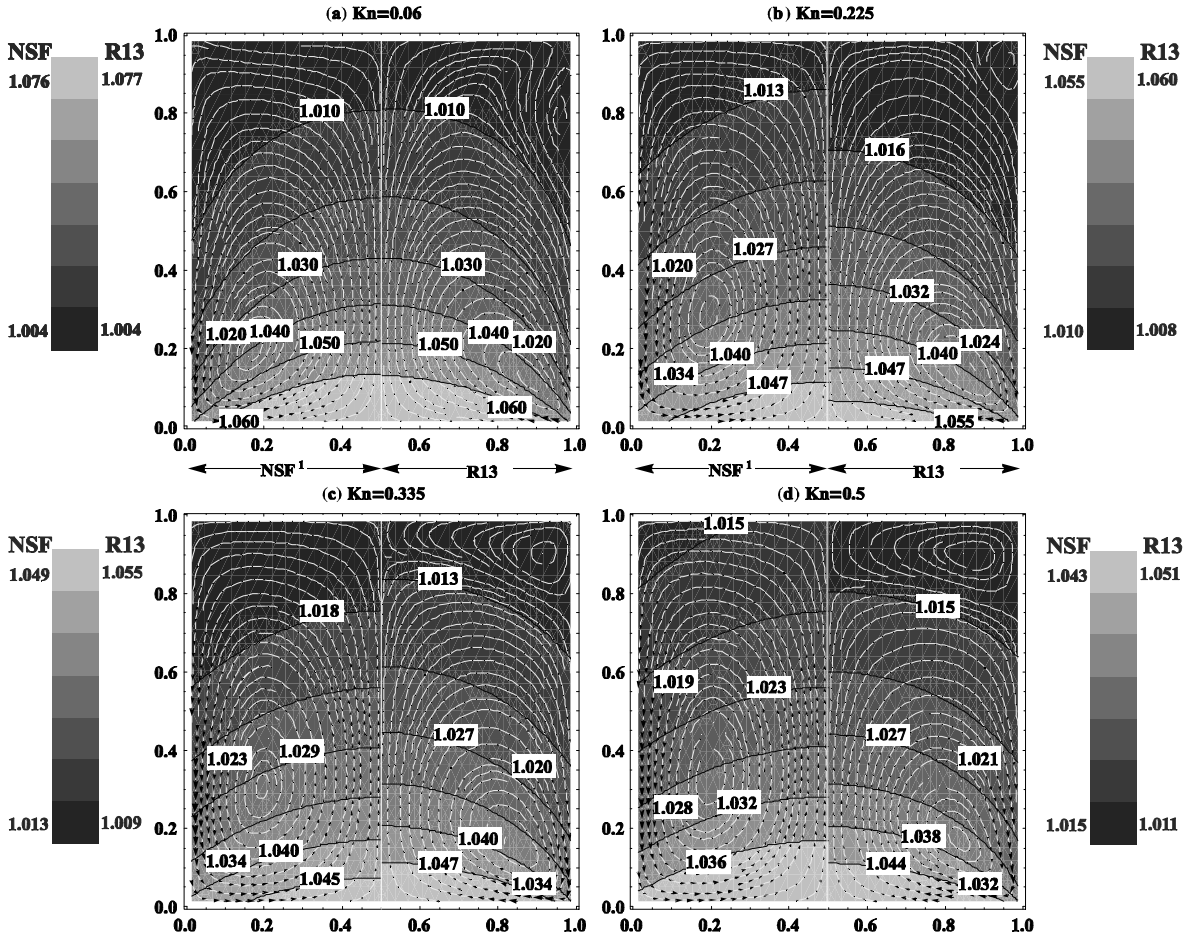

Figure 2. Velocity streamlines and temperature contours for the bottom heated cavity. Temperature ratio is $T_H/T_0 = 1.1$, and Knudsen numbers are 0.06, 0.225, 0.335, and 0.5, in sub-figures (a), (b), (c), and (d), respectively. Results computed with Navier -Stokes-Fourier equations with first order boundary conditions are depicted on the left-half domain, while the results computed with R13 are shown on the right-half portion of the domain.

For the lower portion of the vertical surface ($0 \leq y \lesssim 0.6$), q_y is greater than σ_{xy}, which, according to (11), induces a downward motion in the fluid and thus the primary eddies. However, close to the top plate shear stress dominates over heat flux which produces an upward motion in gas, hence the formation of the secondary vortices. Since the NSF equations overestimate the heat-flux and underestimate the shear stress near the boundary, these secondary eddies do not appear in the Navier-Stokes-Fourier solutions.

For a temperature ratio of 1.1, the magnitude of the dimensionless velocity in the primary and secondary eddies is of the order of 10^{-2} and 10^{-4}, respectively. Both velocities increase slightly with the Knudsen number.

With increasing Knudsen number, all gradients inside the cavity become steeper. Consequently, the secondary eddies becomes more and more pronounced. For Kn$\simeq$ 0.8, the secondary eddies span almost 40% of the cavity area. Although at Kn ≥ 0.5 the results computed with both NSF or R13 equation will be quantitatively different then the more accurate solvers like DSMC, the R13 equations are able to qualitatively predict the behavior of the underlying

process. Moreover, the overall CPU time required for solution of NSF or R13 is far less then for DSMC, especially for slow flows. For example, for a typical case considered in this study, R13 and NSF equations simulation takes about 20 and 12 minutes with an un-optimized matlab code, respectively. On the other hand, a typical DSMC simulation takes about 150 hours [27].

4.2. Heat transfer

Now we will study the effects of rarefaction on the heat transfer from the hot surface, by comparing the results of the NSF and R13 equations, for various Knudsen numbers.

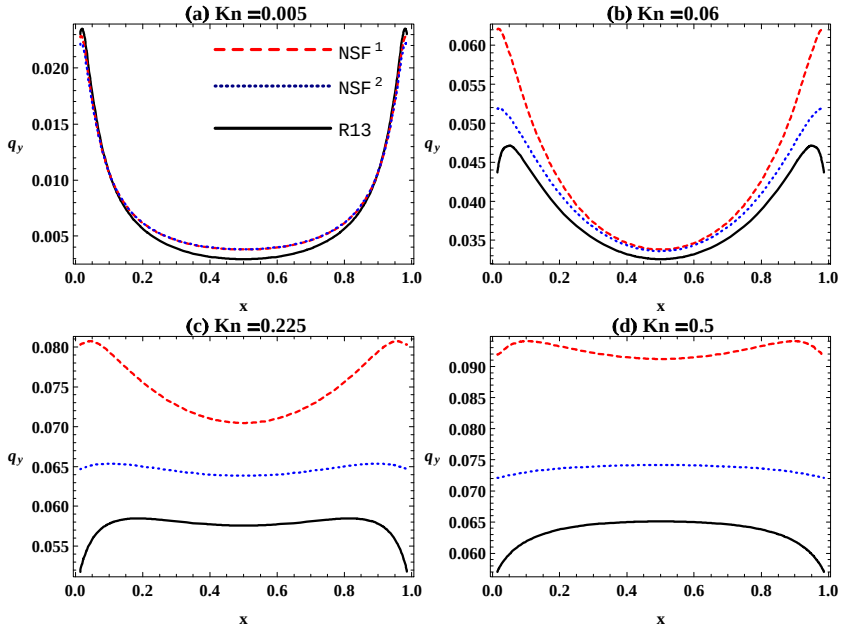

Figure 3. Normal heat flux profiles along the bottom plate, obtained by solving R13 (continuous, black), NSF with first (dashed, red) and second order (dotted, blue) boundary conditions for $Kn = 0.005$, 0.06, 0.225 and 0.5, at tempetature ratio 1.1.

Figure 3 illustrates the variation of the normal heat flux, q_y, along the bottom plate, obtained by solving R13 (continuous, black), NSF (dashed, red) with first order boundary conditions (9) and second order (dotted, blue) boundary conditions (10). At the relatively small Knudsen number 0.005, in Fig. 3(a), all models show good agreement. However at larger Knudsen numbers, in Fig 3(b)-(d), the heat transfer predictions by the classical NSF equations lead to a significant overestimation. This result confirms the conclusion obtained by Liu et al [27] from DSMC computations.

Next, in Fig. 4, we show the net dimensionless heat transfer from the bottom surface, defined as

$$Q_y = \int_0^1 q_y(x,0)dx \ .$$

This is an important quantity for device design, since it describes the thermal performance. Results computed with $T_H/T_0 = 1.1$, using R13 (continuous, black) are compared with NSF with first (dashed, red) and second order (dotted, blue) boundary conditions, are presented in Fig. 4(a). As shown, NSF over-calculates the net heat transfer, however, second order boundary conditions shows a significant improvement over first order boundary conditions.

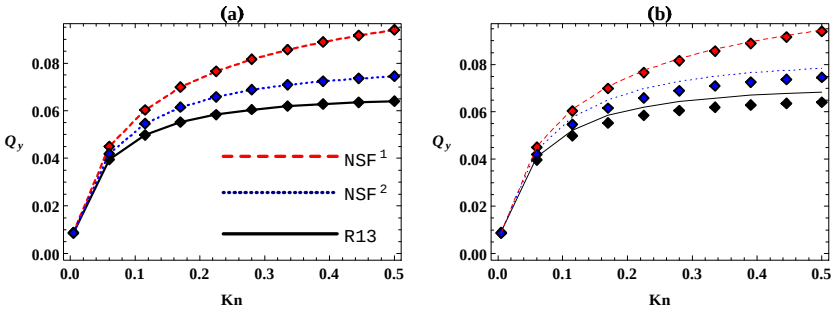

Figure 4. Navier-Stokes results with first (dashed, red) and second order (dotted, blue) boundary conditions are compared with R13 (continuous, black) for various Kn, at temperature ration T_H/T_0 =1.1. In (a), the net heat transfer from the bottom plate is compared between NSF and R13. In (b), the heat transfer through a stationary gas (denoted by curves) is compare against the heat transfer in the moving gas (denoted by symbols, $\diamondsuit$).

To understand the extent to which the convection affects the heat transfer we compute the heat transfer through a stationary gas, where all velocity components vanish, $v_i = 0$, and compare it against the heat transfer in the moving gas, $v_i \neq 0$. Note that this implies a change in boundary conditions, so that no transpiration flow occurs. In an experiment, one will observe the moving gas. As we see from Fig. 4(b), for all continuum models the heat flux from the pure heat conduction is slightly higher than that from the convective heat transfer, the heat transfer is slightly weakened by convection.

5. Conclusions

A numerical investigation of convective heat transfer in a thermal cavity is presented and the influence of the rarefaction effects on the heat transfer in a thermal cavity are studied using Navier-Stokes-Fourier equations with first and second order jump and slip boundary conditions and the R13 equations. It is shown that the NSF equations, with first order boundary conditions, over-estimate the heat transfer, however, second order boundary conditions show an improvement over first order boundary conditions. The R13 results show significant flow patterns which are not present in the NSF equations. This convective mechanism is described in detailed through relative terms in the boundary conditions and their size.

References

[1] Struchtrup H and Torrilhon M 2003 Regularization of Grad's 13 moment equations: Derivation and linear analysis *Phys. Fluids* **15** 2668
[2] Sone Y 2002 *Kinetic Theory and Fluid Dynamics Birkhäuser* (Boston)
[3] Aoki K, Sone Y and Waniguchi Y 1998 A rarefied gas flow induced by a temperature field: Numerical analysis of the flow between two coaxial elliptic cylinders with different uniform temperatures *Computers Math. Applic.* **35**, No. 1/2, 15-28
[4] Sone Y and Yoshimoto M 1997 Demonstration of a rarefied gas flow induced near the edge of a uniformly heated plate *Phys. Fluids* **9** (11)
[5] Struchtrup H and Torrilhon M 2008 Higher-order effects in rarefied channel flows *Phys. Rev.* E **78** 046301
[6] Gad-el-Hak M 2005 *The MEMS Handbook* second edition volumes I–III, (Boca Raton: CRC Press)
[7] Zhang F T, Tang Z, Yu J, and Jin R C 2006 A micro-Pirani vacuum gauge based on micro-hotplate technology *Sensors and actuators A* **126** 300-305
[8] Turnbull H, Barton R C, and Rivire J C 1962 *An Introduction to Vacuum Technique* (Grotge Newnes Limited)
[9] Lee J, Wright T L, Abel M R, Sunden E O and Marchenkov A 2007 Thermal conduction from microcantilever heaters in partial vacuum *J. Appl. Phys.* **101** 014906

[10] Roesle M, Coskun V and Steinfeld A 2011 Numerical Analysis of heat loss from a parabolic trough absorber tube with active vacuum system *J. of Solar Energy Eng.* **133** 031015-1
[11] Hadjiconstantinou N G and Garcia A L 2001 Statistical Error in Particle Simulations of Low Mach Number Flows *Proc. of the First MIT Conf. on Computational Fluid and Solid Mechanics,* Elsevier
[12] Bird G A1994 *Molecular Gas Dynamics and the Direct Simulation of Gas Flows* (Oxford University Press, Oxford)
[13] Radtke G A and Hadjiconstantinou N G 2009 Variance-reduced Particle Simulation of the Boltzmann Transport Equation in the Relaxation-time Approximation *Physical Review* E **79** 056711
[14] Fan J and Shen C 2001 Statistical simulation of low-speed rarefied gas flows *J. Comput. Phys.* **167** 393
[15] Chapman S and Cowling T G 1970 *The Mathematical Theory of Nonuniform Gases* (Cambridge University Press)
[16] Grad H 1949 On the kinetic theory of rarefied gases *Comm.Pure Appl.Math.* 2 p.331-407
[17] Struchtrup H and Torrilhon M 2008 Boundary conditions for regularized 13-moment-equations for micro-channel-flows *J. Comp. Phys.* **227** 1982-2011
[18] Struchtrup H and Taheri P 2011 Macroscopic transport models for rarefied gas flows: A brief review *IMA J. Apppl. Math.* 1-26
[19] Taheri P, Rana A S, Torrilhon M and Struchtrup H 2009 Macroscopic description of steady and unsteady rarefaction effects in boundary value problems of gas dynamics *Continuum Mech. Thermodyn.* **21** 423–443
[20] Taheri P and Struchtrup H 2010 An extended macroscopic transport model for rarefied gas flows in long capillaries with circular cross section *Phys. Fluids* **22** 112004
[21] Taheri P, Torrilhon M and Struchtrup H 2009 Couette and Poiseuille microflows: Analytical solutions for regularized 13-moment equations *Phys. Fluids* **21** 017102
[22] Taheri P and Struchtrup H 2010 Rarefaction effects in thermally–driven microflows *Physica* A **389** 3069–3080
[23] Gu X and Emerson D R 2009 A high-order moment approach for capturing non-equilibrium phenomena in the transition regime *J. Fluid Mech.* **636** 177
[24] Cai C 2008 Heat transfer in vacuum packaged microelectromechanical system devices *Phys. of Fluids* **20** 017103
[25] Sone Y 2009 Comment on "Heat transfer in vacuum packaged microelectromechanical system devices" [Phys. Fluids 20, 017103 (2008)]*Phys. of Fluids* **21** 119101
[26] Sone Y 1985 Boundary temperature effect in a highly rarefied gas *Phys. of Fluids* **28** 419
[27] Liu H, Wang M, Wang J, Zhang G, Liao H, Huang R and Zhang X 2007 Monte Carlo simulations of gas flow and heat transfer in vacuum packaged MEMS devices *Applied Thermal Engineering* **27** 323–329
[28] Papadopoulos D H and Rosne D E 1995 Enclosure gas flows driven by non-isothermal walls *Phys. of Fluids* **7** (11)
[29] Baker J, Calvert M E, Power D J, Chen E T, Ramalingam M L and Lamp T R 1996 On the role of the Knudsen number with respect to heat transfer in micro-scale flows *Proc. of the 31st Intersociety Energy Conversion Eng. Conf.* Vol. **2**, 11-16, pp. 1396-1401
[30] Passian A and Wig A 2002 Knudsen forces on microcantilevers *J. Appl. Phys.* **92** No. 10
[31] Struchtrup H 2005 *Macroscopic Transport Equations for Rarefied Gas Flows* (Springer, New York)
[32] Garcia L, Velasco R M and Uribe F J 2008 Beyond the Navier–Stokes equations: Burnett hydrodynamics *Phys. Rep.* **465** 149
[33] Bobylev A V 2006 Instabilities in the Chapman-Enskog expansion and hyperbolic Burnett equations *J. Stat. Phys.* **124** (2-4) p.371-399
[34] Struchtrup H and Torrilhon M 2008 Higher-order effects in rarefied channel flows *Phys. Rev.* E **78** 046301
[35] Rana A S, Torrilhon M and Struchtrup H 2011A robust numerical method for the R13 equations of rarefied gas dynamics: Application to lid driven cavity (Submitted) *J. Comp. Phys.*
[36] Karniadakis G E and Beskok A 2002 *Micro Flows: Fundamentals and Simulation* (Springer, New York)
[37] Struchtrup H and Torrilhon M 2004 Regularized 13-moment-equations: Shock structure calculations and comparison to Burnett models *J. Fluid Mech.* **513** 171-198
[38] Masters N D and Ye W 2007 Octant flux splitting information preserving DSMC method for thermally driven flows *J Comput. Phys.* **226** pp. 2044-2062